ELSEVIER

Marine and Petroleum Geology 17 (2000) 1085–1093

Marine and Petroleum Geology

www.elsevier.com/locate/marpetgeo

Video cathodoluminescence microscopy of diagenetic cements and its applications

F.W. Witkowski[a], D.J. Blundell[a,*], P. Gutteridge[b], A.D. Horbury[b], N.H. Oxtoby[c], H. Qing[a,d]

[a]*Department of Geology, Royal Holloway, University of London, Egham, Surrey, TW20 0EX, UK*
[b]*Cambridge Carbonates Ltd, 11 Newcastle Drive, The Park, Nottingham NG7 1AA, UK*
[c]*fi[a], 41 Oaken Lane, Claygate, Esher, Surrey KT10 0RG, UK*
[d]*Department of Geology, University of Regina, Regina SK, Canada S4S 0A2*

Received 18 May 2000; received in revised form 31 August 2000; accepted 1 October 2000

Abstract

Diagenetic studies of sedimentary rocks using cold cathodoluminescence (CL) microscopy have been severely limited because of the very low intensity of visible luminescent emissions, which required long photographic exposure times, and because of the difficulty in obtaining quantitative data from CL observations. The solution to this problem is to fit the microscope with a high-sensitivity digital colour video camera linked to a computer with image enhancement and image analysis software. The new technique described in this paper:

- produces digital CL images of consistent high quality, both quickly and cheaply;
- controls the capture and editing of CL images, to reveal detailed textural information even from minerals exhibiting low level luminescence such as quartz;
- acquires quantitative information on pore systems and the abundance of cement zones from CL images.

Examples are presented to demonstrate the high quality of images produced in this way and the range of uses to which the new technique can be applied. The ability to image exactly the same field of view in both plane polarised light and CL is a particular advantage. Image analysis techniques have been developed to give a statistical characterisation of both pore systems and cement phases that infill them. The abundance of contrasting cement zones seen in CL can be measured and the abundance of cement phases can be mapped across a reservoir. The history of porosity occlusion can be reconstructed quantitatively and integrated with burial history and hydrocarbon migration. Porosity can be measured accurately and, since the technique obtains data on pore geometry as well as abundance, the pore system can be characterised by pore size distributions and pseudo-capillary pressure curves. This also opens the possibility of estimating permeability from thin sections.

Keywords: Cathodoluminescence; Image analysis; Carbonate rocks

1. Introduction

Minerals are often precipitated as cement zones within the pore space of a sedimentary rock during diagenesis. For many academic and industrial geological applications, it is useful to determine the sequence and environment of porosity evolution, the relative timing of porosity occlusion and its possible effect on petroleum migration. Analysis requires a wealth of textural information, which was previously obtained using optical examination of stained thin sections (Dickson, 1966), cathodoluminescence (CL) microscopy (Kopp, 1981), and electron microscopy (Grant, 1978; Kearsley & Wright, 1988). These provided qualitative information on the chemical composition, crystal growth forms and relationships between cements, fractures and stylolites, etc. from which the mineral paragenesis could be constructed (e.g. Fairchild, 1983; Frank, Carpenter, & Oglesby, 1982; Grover & Read, 1983; Horbury & Adams, 1989; Kaufman, Cander, Daniels, & Meyers, 1988; Meyers, 1974, 1978; Meyers & Lohmann, 1980; Miller, 1986; Walkden & Berry, 1984).

CL is the emission of visible light (luminescence) by a mineral when bombarded with a beam of electrons in a vacuum chamber (Miller, 1988). The origin of luminescence

* Corresponding author. Tel.: +44-1784-443850; fax: +44-1784-471780.
E-mail addresses: francis@gl.rhbnc.ac.uk (F.W. Witkowski), d.blundell@gl.rhbnc.ac.uk (D.J. Blundell), pete@caco3.demon.co.uk (P. Gutteridge), oxtoby@dial.pipex.com (N.H. Oxtoby), hairuo.qing@uregina.ca (H. Qing).

0264-8172/00/$ - see front matter
PII: S0264-8172(00)00055-6

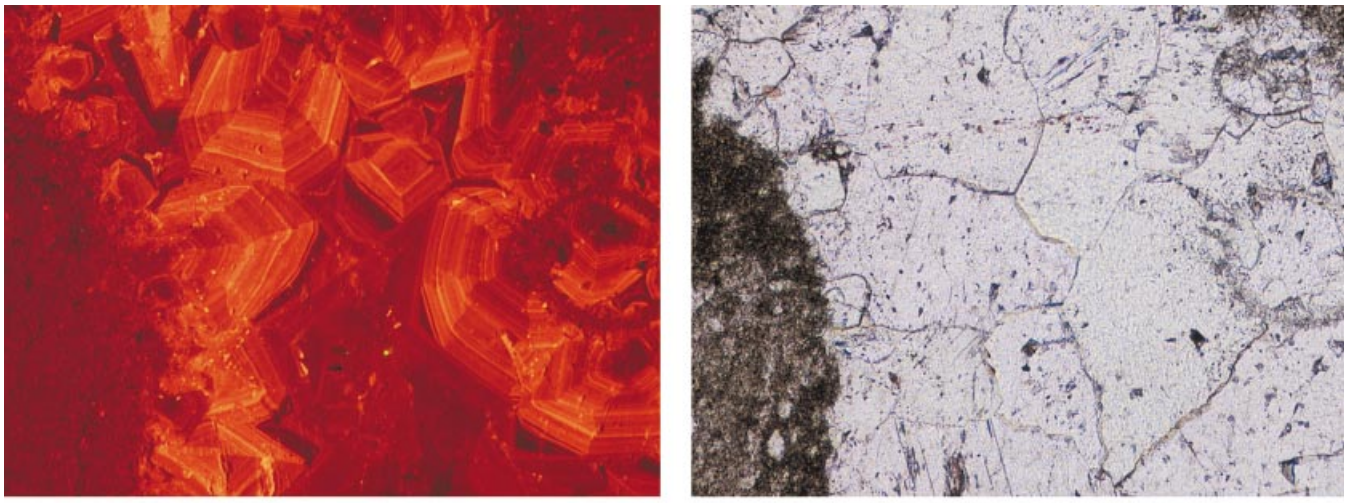

(a) (b)

Fig. 1. (a) CL image of diagenetic calcite cements in a limestone showing concentric orange–yellow bands of growth zonation and radiating facets of sector zonation. (b) Same image in transmitted light. Devonian, western Canada. F.oV. 2.8 mm × 2.1 mm.

is accepted as being due to trace elements incorporated into the crystal lattice during growth or the presence of lattice defects (Fairchild, 1983; Frank et al., 1982; Habermann, Neuser, & Richter, 1998; Machel, 1985; Pierson, 1981; Savard, Veizer, & Hinton, 1995; ten Have & Heijnen, 1985). In cold CL microscopy, a polished thin section is placed in a small vacuum chamber and is bombarded with low energy (10–20 kV) electrons. The instrumentation required is readily available. Visible emissions emanating from trace elements or mineral defects are conventionally observed through an optical microscope. These can be readily observed in carbonates because of the relatively low energy of electrons required to excite luminescence. CL colours depend largely on the trace element or defect responsible for the emission and the mineral host. Luminescence of carbonates is controlled by the relative abundance of Fe^{2+} and Mn^{2+} in the crystal lattice (e.g. Machel, 1985; Savard et al., 1995). Luminescence of calcite is generally orange, whilst dolomite is red. The phenomena of growth zonation and sector zonation can be observed in carbonates using CL. Growth zonation occurs when pore fluid composition and/or Eh–pH values change during precipitation (Meyers, 1974, 1978; Meyers & Lohmann, 1980), giving rise to concentric light and dark banding as shown in Fig. 1a. Sector zonation (e.g. Reeder & Grams, 1987; Reeder & Paquette, 1989; Reeder & Prosky, 1986) occurs when growing faces of a mineral with different crystallographic orientations incorporate different concentrations of trace elements,

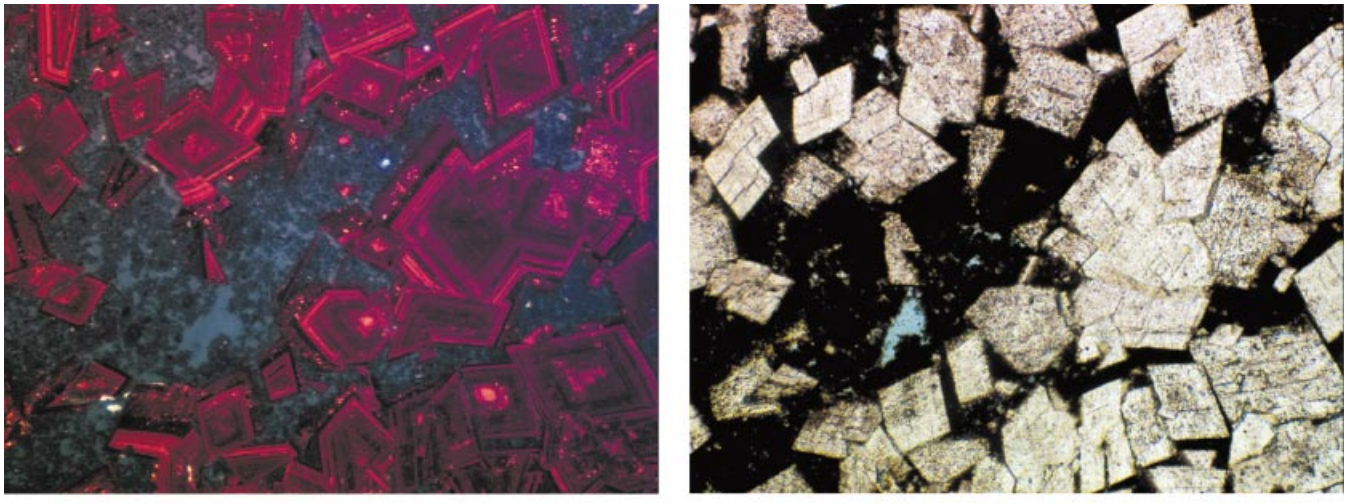

(a) (b)

Fig. 2. (a) CL image of dolomite rhombs showing concentric growth zonation. (b) Same image in transmitted light. The black areas are hydrocarbon and the blue is void filled with resin when preparing the slide. Upper Devonian, western Canada. F.oV. 1.5 mm × 1.125 mm.

as shown in Fig. 1a by the facets of differing colour tones in the cements surrounding the mineral grains.

The intensity of luminescence from quartz is too low to be visible with conventional cold CL microscopy using an optical microscope, but can be observed using hot CL microscopy, in which the cathode element is heated in a high vacuum to produce higher energy electrons. Hot CL microscopy has the advantage that colour luminescence images are readily seen in quartz. However, it is little used because the more flexible, and commercially available, scanning electron microscope (SEM), fitted with a CL detector, produces comparable results and is generally preferred. SEM gives only greyscale CL images, which are less useful, although spectral information can be acquired. The controls on quartz luminescence are poorly understood, although the presence of aluminium as a trace element or crystal defects produced by water molecules may be an important factor (Marshall, 1988; Miller, 1986). Cold CL microscopy has therefore been preferred for carbonates, whereas SEM or hot CL microscopy were preferred for silicates.

Conventionally, standard optical microscopy and photographic techniques have been used to observe and record CL. Because of the very low intensity of visible luminescent emissions, subtle variations can be difficult to detect by eye. It can be a painstaking process to examine a thin section and information can be lost because the light intensity is too low to be discernible, even when working in a darkened room. Photography requires long exposure times and has a number of disadvantages, such as the inability to control image quality during exposure, the inability to edit or enhance the image once it has been obtained and the expense of film processing. These can be overcome by replacing the photographic camera with an image enhancing, digital video camera. The method of digital image capture and editing described here allows the observer considerable control over the image quality both during and after capture. First, the luminescent image of a thin section is obtained in real time and can be seen clearly on a computer screen, so that adjustments can be made during the observation. Secondly, following capture, the image can be edited to emphasise selected features. The problem of observing low intensity luminescence from minerals such as quartz and "non-luminescent" carbonates is also overcome by this technique since the image capture process is interactive and low intensity luminescence can be considerably enhanced. This is particularly important for studies involving quartz since this technique obviates the need to use a hot cathode luminoscope. The almost instantaneous image capture means that transient luminescence such as shown by kaolinite or barite and, indeed, many resins used for impregnating the pore space, can be imaged readily.

2. Materials and methods

Two sets of imaging equipment were utilised in this study: a Hamamatsu 5810 chilled 3-colour CCD (charged coupled device) camera, with 752×508 pixel resolution and a DataCell Snapper board, and a Photonic Science 3CCD peltier-cooled camera, with 732×582 pixel resolution and a Matrox Meteor framegrabber. These are controlled by Image Pro Plus 4.1 image processing and analysis software. The camera is mounted on a Nikon Optiphot petrological microscope fitted with a Technosyn 8200 MkII luminoscope to produce the electron beam. Instruments with comparable specifications are available from other manufacturers. Images are collected by controlling the 3CCD camera with the computer software and storing the image data as TIFF files. They can then be printed on a suitable inkjet or video printer, recalled to screen or incorporated into multimedia displays. Image acquisition operates in two modes: a "snapshot" facility, similar to a conventional camera, which is useful for straightforward PPL transmitted light images, and an integration mode. The latter uses the framegrabber to combine images in order to obtain optimum image quality for CL visualisation. In principle, several thousand images can be stacked, although it has never been found necessary to exceed 250 images or 30 s of integration time.

Once acquired, a range of image processing and analysis functions can be applied to the images. Image sharpening accentuates detail by employing a convolution process that removes blurring from the original image. This is achieved with a single pass, 3×3 kernel. A generally useful technique is to apply Boolean operators to images of the same field of view taken under different conditions. For example, passing transmitted light through geological thin sections often produces an extremely wide intensity range, so that some portions of an image are underexposed and others are overexposed. By obtaining both a slightly overexposed and a slightly underexposed image of the same field of view, and applying an averaging operator, an image that is almost perfectly exposed throughout can be obtained. Further processing techniques to improve image quality include a display range option that increases contrast and enhances brightness in low light situations. Another useful enhancement is to increase dark area contrast by use of a non-linear contrast correction factor that is then applied to the image. Known as a (LUT) gamma function, this operates by altering mid-tone values, especially the low end ones, without affecting highlight and shadow points. However, the main advantage of this technique over pre-existing systems is that CL emission from almost any geological material can be imaged accurately and quickly on one instrument. CL emissions are often very faint and subtle variations can be difficult to detect by eye, even when viewed in a completely darkened room. With photography, long exposure times are required, even when using fast film. Because of this, reciprocity failure can occur, where colours are inaccurately registered. Using a digital camera there is no perceptible reciprocity failure when comparing the luminescence viewed through the microscope eyepieces with the on-screen image. It is not possible to judge whether failure occurs when

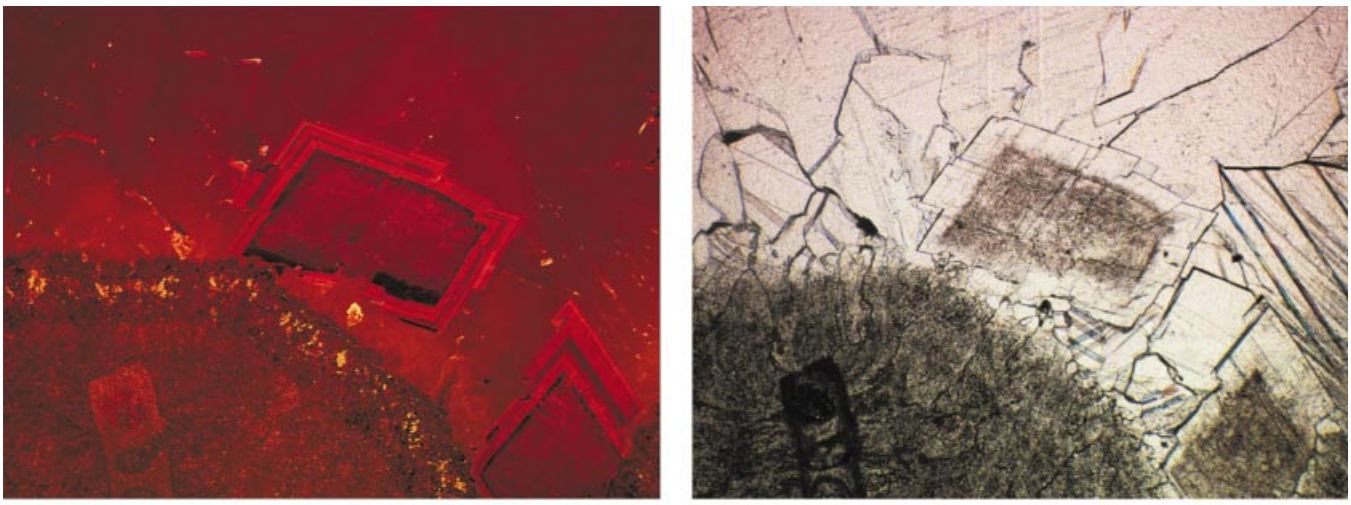

Fig. 3. (a) CL image of saddle dolomite crystals, showing growth zonation, nucleated on the surface of marine cryptofibrous calcite cement. The remaining porosity is infilled with dull luminescent calcite with broad zones. (b) Same image in transmitted light. Permian bioherm, Barents Shelf. F.oV. 2.9 mm × 2.2 mm.

luminescence images are captured at the lowest intensity levels that are barely discernible visually, e.g. for some types of sandstone. However, images captured digitally from sandstones are similar in appearance and colour range to those obtained photographically from hot CL microscopy.

3. Mineral imaging

CL and transmitted light images of a thin section of diagenetic calcite cements in a limestone are shown in Fig. 1. The CL image, Fig. 1a, is the result of integrating a stack of 15 images and shows an example of classic orange–yellow growth and sector zonation in calcite as a result of variations in the relative abundance of Fe^{2+} and Mn^{2+} in the crystal lattice (e.g. Machel, 1985; Savard et al., 1995). This is regarded as due to variation in relative abundance of Fe^{2+} and Mn^{2+} in the crystal lattice of the calcite, formed during growth. The banding is invisible on the transmitted light image, Fig. 1b. The luminescence intensity of

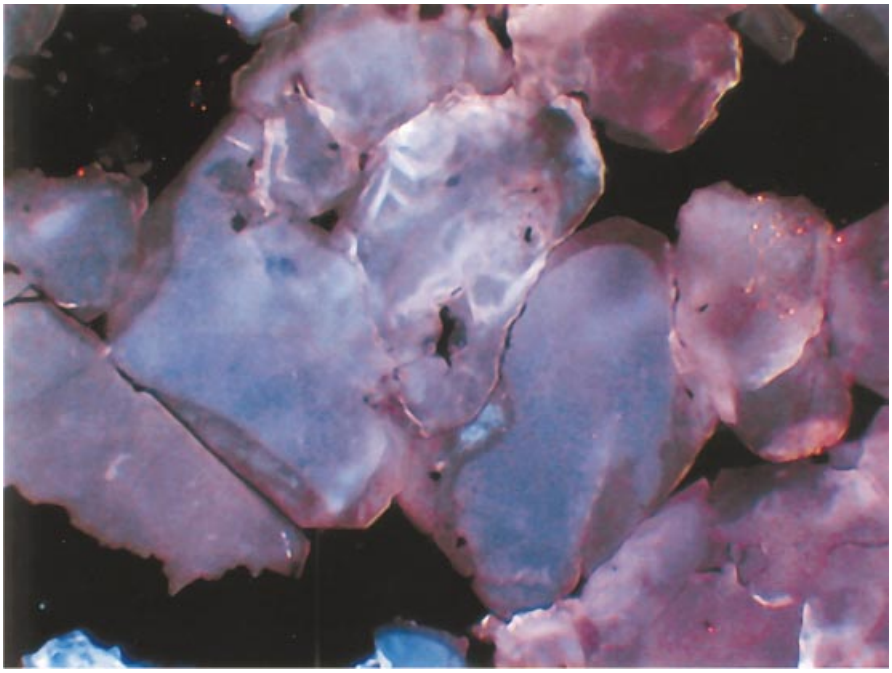

Fig. 4. CL image of sandstone showing moderately luminescent pale blue quartz grains with purple–brown luminescent diagenetic cement overgrowths. Intergranular porosity is black. Jurassic, Norwegian Shelf. F.oV. 1.5 mm × 1.125 mm.

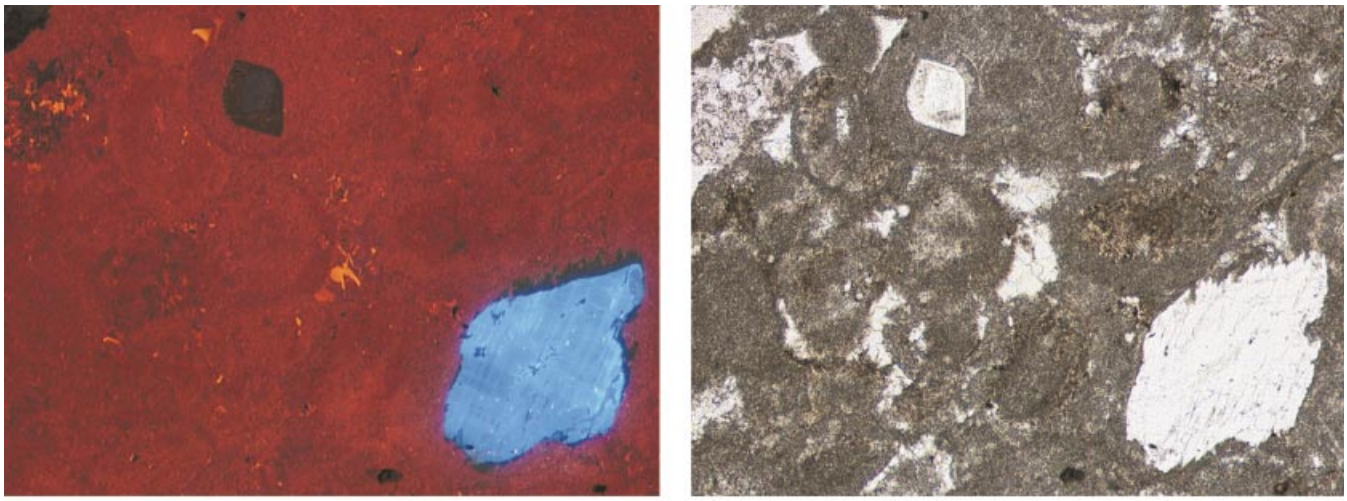

Fig. 5. (a) CL image of an oolitic limestone containing a luminescent bright blue detrital microcline feldspar grain rimmed with a dark blue–black overgrowth. The ooids have a uniform orange–brown luminescence; intergranular pore space is infilled with zoned calcite cement. (b) Same image in transmitted light. Jurassic, Mexico. F.oV. 1.4 mm × 0.95 mm.

this sample is typical of many limestones, and the image could have been collected photographically. Using a digital camera system, however, it is possible to optimise on-screen the image of a desired feature in the field of view, such as the fine scale growth zonation banding.

CL and transmitted light images of diagenetic dolomite are presented in Fig. 2. The CL image, Fig. 2a, is also the integration of 15 images, and shows the concentric reddish growth zonation characteristic of this mineral. The banding is also visible in transmitted light, Fig. 1b, as diffuse zones of inclusions. The origin of the luminescence can be explained in the same way as for the calcite shown in Fig. 1a — the mineral environment alters the luminescence emission.

CL and transmitted light images of diagenetic saddle dolomite crystals and calcite cements in a limestone are presented in Fig. 3. The CL image, Fig. 3a, shows growth zonation around the rims of the saddle dolomite crystals, but this is invisible in transmitted light, Fig. 3b. The luminescence of this sample is almost invisible to the eye, and photography might not have been attempted. By integrating 40 images, the zonation is imaged as effectively as in Fig. 1a.

A CL image of diagenetic quartz cements in a sandstone is presented in Fig. 4. In some sandstones, for reasons that are unclear, luminescence is observable by eye using cold CL and is readily photographed. However, the majority of sandstones show little visible luminescence and, conventionally, visualisation would have required hot CL or SEM-CL. For example, the pale blue and purple–brown luminescence shown in Fig. 4 is invisible to the eye, even in a completely darkened room. This image was produced by integrating 180 images, and shows differentiation of the less luminescent grains from the more luminescent overgrowths: the overgrowths are a darker purple brown while the detrital grains are shades of pale blue. It illustrates the effectiveness of cold CL digital microscopy for imaging silicate rocks, and its clear advantages over hot CL or SEM-CL.

Fig. 5 illustrates the power of CL imagery to illuminate details that cannot be observed with transmitted light. The CL image, Fig. 5a, shows that the majority of this rock is composed of orange–brown luminescent calcite ooliths. The luminescent bright blue detrital feldspar grain shows faint crosshatch twinning, which indicates that it is microcline. The thin dark blue–black rim surrounding this grain is an authigenic feldspar overgrowth. Kaolinite fracture fills are shown in Fig. 6 to illustrate how the transient CL of

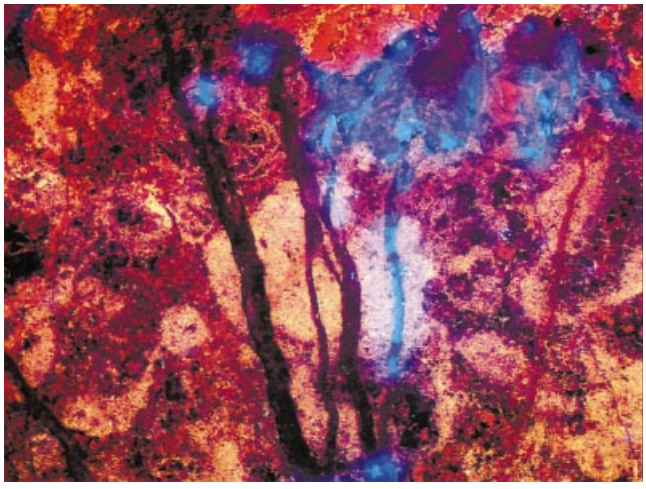

Fig. 6. CL image of a carbonate breccia. Fractures filled with carbonate have a dull luminescence in shades of brown. Fractures filled with kaolinite show a spectacular blue luminescence, which is transient but can be captured by this technique because of the short time required to obtain the image. Cretaceous, southern Italy. F.oV. 1.5 mm × 1.125 mm.

kaolinite can be easily obtained using the rapid integration of the digital image capture technique. Images of transient CL are extremely difficult to obtain by conventional photography as the kaolinite CL signature fades rapidly under the electron beam.

Figs. 1–6 were all obtained with a CL microscope coupled with a digital image capture, enhancement and analysis system. The suite of digital images that can now be acquired, together with image analysis software, provides the basis for generating abundance and geometrical data on both pore systems and cement zones as revealed by CL.

4. Porosity measurement

Using images of thin sections, porosity can be estimated in two main ways: from transmitted light microscopy and from CL microscopy. For use in transmitted light, dyes with a contrasting colour to the rock (e.g. Sudan blue) are mixed with the mounting resin so that pores are readily distinguished, as shown in a partly dolomitised ooid grainstone, Fig. 7b. Computer images are then segmented to isolate the porosity using, for example, the RGB histograms or colour cube model, and standard object analysis algorithms are applied to obtain the measurement. Under CL, resins are either completely non-luminescent (i.e. black, Fig. 7a) or show transient blue luminescence, and the same procedure as in transmitted light can be applied to CL images to isolate and measure the porosity. There are advantages and disadvantages to both routes. CL is a surface technique so that pore boundaries are sharply resolved, but complete non-luminescence can also occur in calcite and quartz cements so that segmentation of porosity may require considerable intervention by the observer. Conversely, transmitted light provides an image through approximately 30 μm of rock so that pore boundaries are often represented by a diffuse band rather than a sharp line, Fig. 7b, leading to measurement errors. In practice, CL images are generally more successful for porosity segmentation with dolomites whilst transmitted light images are better for limestones and sandstones. However, there are occasions when the reverse is true and this depends upon the relative quality of individual CL–PPL image pairs.

A major application of this technique is to obtain quantitative data on the pore system and abundance of cement zones or replacement minerals such as dolomite. The original CL image (Fig. 7b) has been segmented to identify the non-luminescent porosity (Fig. 7c) and red luminescent dolomite (Fig. 7d) so that their distribution and abundance can be determined. Measuring abundance data of CL phases by image analysis is considerably more accurate and much less time consuming than attempting to obtain the same data from conventional photomicrographs. A number of workers have shown that image analysis of SEM and thin section images can successfully provide additional data for both total porosity and pore geometry (Bowers, Carr & Murray, 1998; Carr & Paschke, 1998; Dorobek, Read, Niemann, Pong, & Haralick, 1987). This is an important way of obtaining porosity data for the oil industry. It is particularly useful when core plugs cannot be cut, for example where core recovery is poor, only sidewall cores or cuttings are available, when only a limited amount of old core material survives, or when it is necessary to sample specific types of pore space such as matrix porosity in fractured reservoirs. The use of digitally acquired CL and PPL images of exactly the same field of view enables more efficient image analysis, for a wide range of material. An attempt has been made to find a set of functions based on image analysis parameters that are accurate and robust predictors of core plug porosity and permeability. An intelligent predictive algorithm (Saunders, Gammerman, & Vovk, 1998) was applied to various sets of image analysis statistical attributes, that included pore size distributions, roundness, pore perimeter, etc. This attempted to predict porosity and permeability from a series of core plugs, for which the measured values were known. The program operates on a “training” dataset in such a way that it can “learn” an optimum set of weighting coefficients. These are combined with attributes in a non-linear multivariate analysis, in order to give the best prediction of the desired value — in this case the measured porosity or permeability. As such, it is a generalisation of standard neural network methods. Non-linear statistical analysis using this program proved valuable as a predictive tool for porosity. As well as giving excellent predictions, it also provides a quantitative estimate of the accuracy of the predictions. However, this technique is presently less successful in predicting permeability. Fig. 8 shows the correlation between porosity predicted from image analysis of thin sections and porosity measured on plugs using the standard helium porosimetry method, based on 53 samples from a large number of locations, including both limestones and dolomites. The average difference between them is 1.86% with 33 samples individually within 2%.

A further advantage of this method is the ability to examine the pore size distribution and to measure the amount of porosity carried by the pores within any particular size range, although within the limits of a thin section. Fig. 9 shows the variation of porosity with pore size for five samples chosen to represent a range of porosities. For these samples, the bulk of the porosity is contained within the larger sized pores.

5. Discussion

Figs. 1–6 illustrate the major improvement in imagery that can be obtained from CL microscopy through the use of a digital camera linked to a computer with software for image enhancement, processing and analysis. The improvement in quality and range of images, the ability to image identical areas of a thin section under plane polarised light

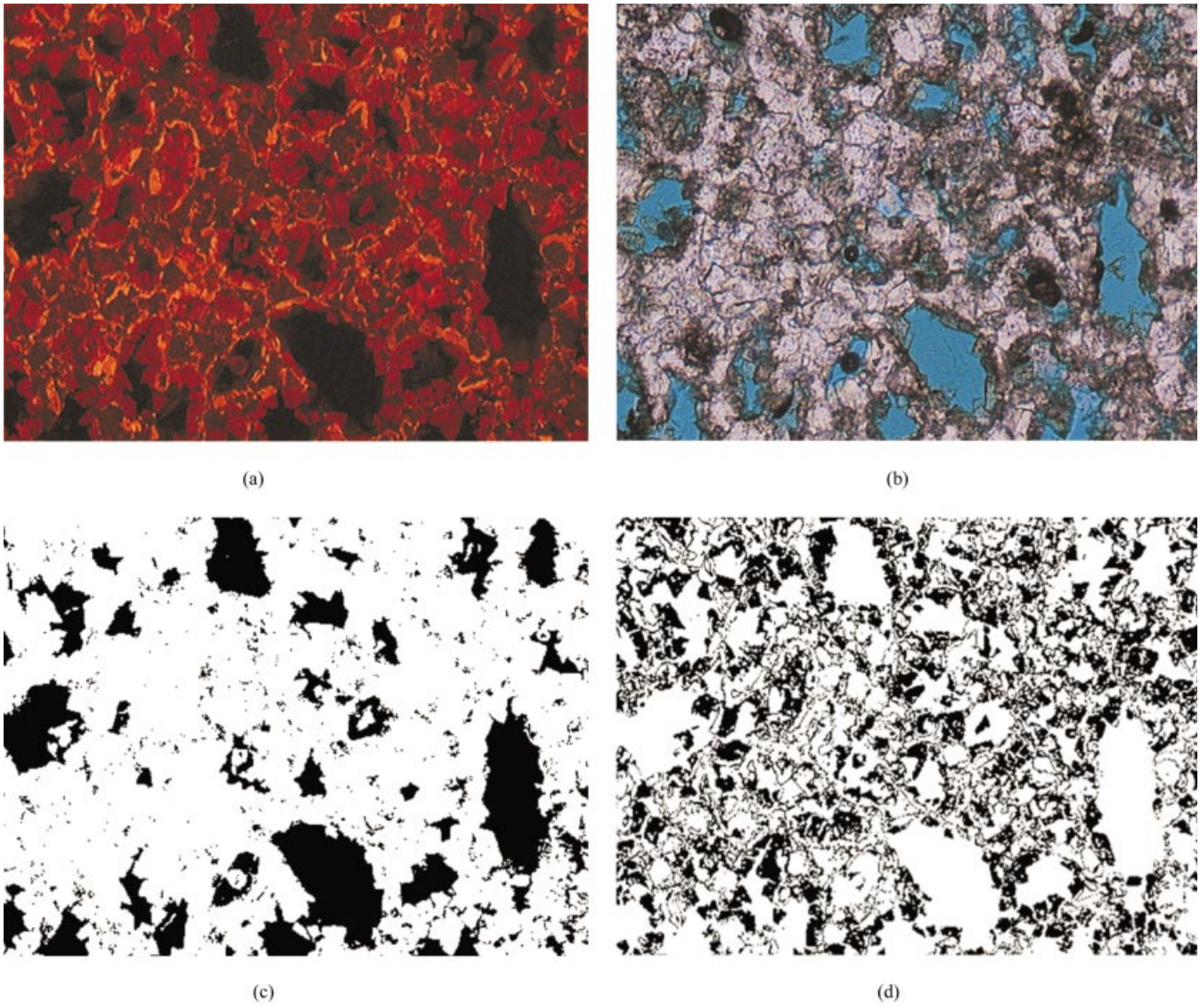

Fig. 7. (a) CL image of a partly dolomitised ooid grainstone. (b) Same image in transmitted light. Pores show as black areas on the CL image and as pale blue in transmitted light. (c) CL image segmented so that the pore system is picked out in black. It is largely oomouldic with minor intergranular and intercrystalline pores, total porosity is 23.54%. (d) CL image segmented so that the replacement mineral dolomite has been picked out in black. 38.23% dolomite is present. Roker Dolomite, Sunderland. F.oV. 1.25 mm × 0.85 mm.

and CL, and the ability to acquire quantitative information about the images are providing opportunities to enhance and extend the range of applications. At present, the full extent of these is still being explored and techniques are being developed accordingly.

An important potential application of this technology is the quantification of the growth stages of diagenetic cements — how much cement is precipitated in a particular time interval, and what is its distribution across an area? Horbury, Celestino, Oxtoby, Soto, and Johnson (1996) presented results of a successful exercise of this nature, performed manually, in which CL photographs were digitised to determine the relative abundance of different cement zones. Using the new technology described in this paper, the image analysis process can at least be semi-automated.

CL images are segmented, divided into discrete areas on-screen by the observer, after which algorithms calculate the areas. Difficulties arise in full automation based on segmentation of colour-intensity variation because different growth stages may have similar colours, although they can be distinguished by pattern or size. Accordingly, various automated pattern recognition algorithms are being investigated. Furthermore, it should be possible to quantify, or numerically characterise, the classification scheme of Lucia (1995, 1999). This would aid the prediction of permeability by finding the critical parameters that can be obtained from image analysis that will define, for example, the relationships between fracture, intergranular and mouldic pore space.

Although porosity and pore space characteristics are

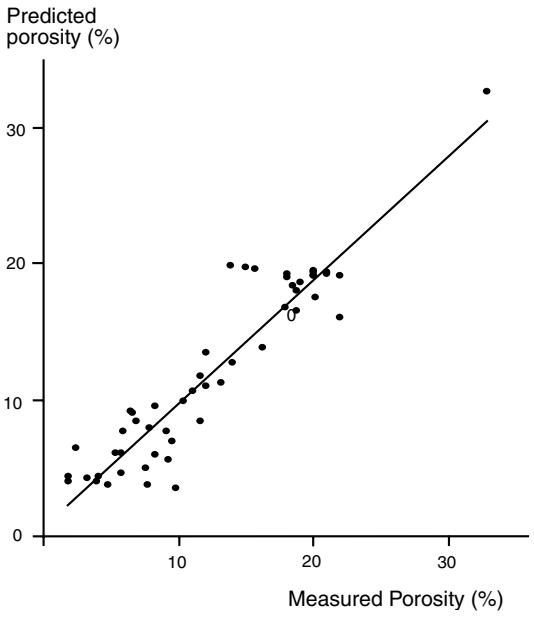

Fig. 8. Correlation between porosity predicted from image analysis of thin sections and bulk porosity measured on plugs of 53 samples of limestone and dolomite from a wide range of localities.

demonstrably predictable with the technology described above, there remains a need to integrate it with recent mathematical research directed at generalising neural network algorithms, in order to predict permeability from image analysis data. Permeability prediction from images has been attempted by a number of workers, applying a diversity of mathematical methods, with varying degrees of success. Ehrlich, Etris, Brumfield, Yuan, and Crabtree (1991), who reported the most accurate predictions published so far, considered that, for practical purposes, by the time a prediction has been proved successful, the need for it has largely gone. This view may have been overtaken by recent developments in mathematics and computing power, which could make the goal of a useful permeability prediction again a feasible proposition. The problem is not easy to resolve, and may even prove to be intractable, but at least needs to be attempted.

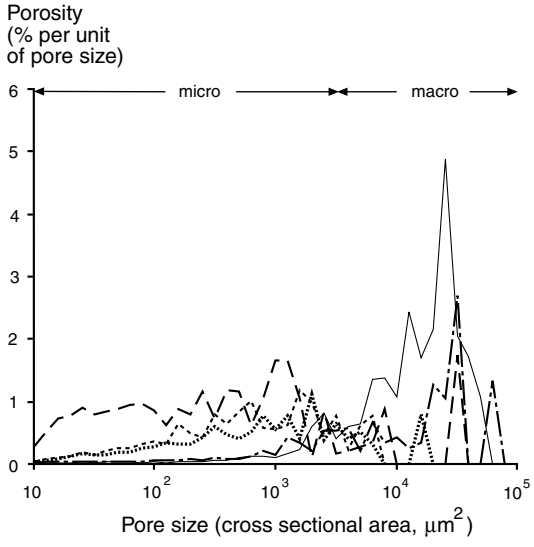

Fig. 9. Plot of porosity distribution versus pore size (cross-sectional area on thin section) for five representative limestone samples. Porosity is shown as % per pore size unit where each unit is $\log_{10}$ (pore size) = 0.1.

Finally, the image analysis techniques developed to characterise CL images of thin sections, described above, can be adapted for other kinds of images: for example scaled upwards to analyse core photos, image logs and even outcrop-scale features. This extends both the range of scales and the range of applications of the image analysis techniques.

Acknowledgements

This research formed part of a project within the LINK Hydrocarbon Reservoirs programme funded by DTI and NERC, together with BG plc, PetroCanada Oil and Gas and Shell International Exploration and Production, to all of whom we express our sincere gratitude. We thank Professor A Gammerman and Mr C Saunders for their advice on numerical analysis of the image data and for providing a working copy of their “Ridge Regression” program. We also thank Professor J Gluyas and an anonymous referee for helpful and stimulating comments.

References

Bowers, M. C., Carr, M. B., & Murray, C. J. (1998). Correlation of porosity types derived from NMR data and petrographic image analysis. *Abstracts, American Association of Petroleum Geologists Annual Convention.* Salt Lake City, Utah, 17–21 May.

Carr, M. B., & Paschke, C. A. (1998). Spatial analysis of fabric elements in the Berea sandstone through petrographic image analysis. *Abstracts, American Association of Petroleum Geologists Annual Convention*. Salt Lake City, Utah, 17–21 May.

Dickson, J. A. D. (1966). Carbonate identification and diagenesis as revealed by staining. *Journal of Sedimentary Petrology*, *36*, 491–505.

Dorobek, S. L., Read, J. F., Niemann, J. M., Pong, T. C., & Haralick, R. M. (1987). Image analysis of cathodoluminescent-zoned calcite cements. *Journal of Sedimentary Petrology*, *57*, 766–770.

Ehrlich, R., Etris, E. L., Brumfield, D., Yuan, L. P., & Crabtree, S. J. (1991). Petrography and reservoir physics III: physical models for permeability and formation factor. *American Association of Petroleum Geologists Bulletin*, *75*, 1579–1592.

Fairchild, I. J. (1983). Chemical controls of cathodoluminescence of natural dolomites and calcites: new data and review. *Sedimentology*, *30*, 579–583.

Frank, J. R., Carpenter, A. B., & Oglesby, T. W. (1982). Cathodoluminescence and composition of calcite cement in Taum Sauk limestone (Upper Cambrian), southeast Missouri. *Journal of Sedimentary Petrology*, *52*, 631–638.

Grant, P. (1978). The role of the scanning electron microscope in cathodoluminescence petrology. In W. B. Whalley (Ed.), *Scanning electron microscopy in the study of sediments* (pp. 1–11). Geo Abstracts, Norwich, UK.

Grover Jr, G., & Read, J. F. (1983). Paleoaquifer and deep burial related cements defined by regional cathodoluminescent patterns, Middle

Ordovician carbonates, Virginia. *American Association of Petroleum Geologists Bulletin*, *67*, 1275–1303.

Habermann, D., Neuser, R. D., & Richter, D. K. (1998). Low limit of Mn^{2+}-activated cathodoluminescence of calcite: state of the art. *Sedimentary Geology*, *116*, 13–24.

Horbury, A., Celestino, J. L., Oxtoby, N. H., Soto, A., & Johnson, S. (1996). Diagenesis y evolucion de la porosidad en el campo petrolifero Arenque, costa afuera de Tampico, Tamaulipas, Mexico. *Boletin de la Asociacion de los Geologos Petroleros Méxicanos*, *45*, 58–80.

Horbury, A., & Adams, A. E. (1989). Meteoric phreatic diagenesis in cyclic Late Dinantian carbonates, northwest England. *Sedimentary Geology*, *65*, 319–344.

Kaufman, J., Cander, H. S., Daniels, L. D., & Meyers, W. J. (1988). Calcite cement stratigraphy and cementation history of the Burlington–Keokuk formation (Mississippian), Illinois and Missouri. *Journal of Sedimentary Petrology*, *58*, 312–326.

Kearsley, A., & Wright, P. (1988). Geological applications of scanning cathodoluminescence imagery. *Microscopy and analysis*, September, 3 pp.

Kopp, O. C. (1981). Cathodoluminescence petrography, a valuable tool for teaching and research. *Journal of Geological Education*, *29*, 108–113.

Lucia, F. J. (1995). Rock fabric/petrophysical classification of carbonate pore space for reservoir characterization. *American Association of Petroleum Geologists' Bulletin*, *79*, 1275–1300.

Lucia, F. J. (1999). *Carbonate reservoir characterization*, Berlin: Springer (226 pp.).

Machel, H. G. (1985). Cathodoluminescence in calcite and dolomite and its chemical interpretation. *Geoscience Canada*, *12*, 139–147.

Marshall, D. J. (1988). *Cathodoluminescence of geological materials*, London: Unwin Hyman Ltd (146 pp.).

Meyers, W. J. (1974). Carbonate cement stratigraphy of the lake valley formation (Mississippian), Sacramento Mountains, New Mexico. *Journal of Sedimentary Petrology*, *44*, 837–861.

Meyers, W. J. (1978). Carbonate cements: their regional distribution and interpretation in Mississippian limestones of southwestern New Mexico. *Sedimentology*, *25*, 371–400.

Meyers, W. J., & Lohmann, K. C. (1980). Geochemistry of regionally extensive calcite cement zones in Mississippian skeletal limestones, New Mexico. *Bulletin of the American Association of Petroleum Geology*, *65*, 597–628.

Miller, J. (1986). Facies relations and diagenesis in Waulsortian mudmounds from the Lower Carboniferous of Ireland and N. England. In J. H. Schroeder & B. H. Purser, *Reef diagenesis* (pp. 311–335). New York: Springer.

Miller, J. (1988). Cathodoluminescence microscopy. In M. Tucker, *Techniques in sedimentology* (pp. 174–190). Oxford: Blackwell Scientific.

Pierson, B. J. (1981). The control of cathodoluminescence in dolomite by iron and manganese. *Sedimentology*, *28*, 601–610.

Reeder, R. J., & Grams, J. C. (1987). Sector zoning in calcite cement crystals: implications for trace element distributions in carbonates. *GCA*, *51*, 187–194.

Reeder, R. J., & Paquette, J. (1989). Sector zoning in natural and synthetic calcites. *Sedimentary Geology*, *65*, 239–247.

Reeder, R. J., & Prosky, J. L. (1986). Compositional sector zoning in dolomite. *Journal of Sedimentary Petrology*, *56*, 237–247.

Saunders, C., Gammerman, & A., Vovk, V. (1998). Ridge regression algorithm in dual variables. In J. Shavik (Ed.), *Proceedings of the Fifteenth International Conference*, ICML98.

Savard, M. M., Veizer, J., & Hinton, R. (1995). Cathodoluminescence at low Fe and Mn concentration: a SIMS study of zones in natural calcites. *Journal of Sedimentary Research*, *A65*, 208–213.

ten Have, T., & Heijnen, W. (1985). Cathodoluminescence activation and zonation in carbonate rocks: an experimental approach. *Geologie en Mijnbouw*, *64*, 297–310.

Walkden, G. M., & Berry, J. R. (1984). Natural calcite in cathodoluminescence: crystal growth during diagenesis. *Nature*, *308*, 525–527.